Textures and Microstructures, 1997, Vol. 29, pp. 103–126
Reprints available directly from the publisher.
Photocopying permitted by license only

MODEL CALCULATIONS OF THE ACCURACY OF STRUCTURE FACTOR DETERMINATION FROM TEXTURED POWDER SAMPLES

R. HEDEL, H. J. BUNGE and G. RECK

Department of Physical Metallurgy, Technical University of Clausthal, Grosser Bruch 23, D-38678 Clausthal-Zellerfeld, Germany; Federal Institute of Materials Research and Testing, Berlin, Germany

(Received 23 January 1997)

Crystal structure analysis is based on absolute values of structure factors $|F_{hkl}|$. These values can be measured by powder diffraction. In random powder diffraction many superpositions occur in the diffraction diagram over the Bragg angle θ. If non-random (textured) samples are used and intensity measurements are done in the three-dimensional reciprocal space, i.e. over θ and the sample rotation angles $\alpha\beta$, then these superpositions can be deconvoluted to a good deal. In order to perform this deconvolution a two-step procedure was developed and was implemented in a computer code. In the first step the texture is determined from a low number of reflections having no or only two-fold overlap. In the second step the deconvolution is done for all reflections. This includes the deconvolution of "systematically" overlapped reflections, e.g. those with the same $h^2+k^2+l^2$ in cubic symmetry.

Model calculations were performed in order to test the reliability and resulting accuracy of the deconvolution procedure depending on various experimental as well as modelling parameters. It is concluded that good resolution for superposed $|F_{hkl}|$ can be reached up to reasonably high lattice parameters.

The decisive accuracy limiting factor is texture determination in the first step of the procedure. It is concluded that it is necessary to employ texture analysis methods with higher angular resolving power and higher statistical accuracy than in conventional routine texture analysis. This is, however, possible with the existing modern texture diffractometers.

KEY WORDS: Crystal structure analysis; Three-dimensional intensity distribution functions; Peak overlap; Deconvolution

INTRODUCTION

Crystal structure analysis is the determination of atom positions in the unit cell of the crystal lattice. The atom positions are obtained from the electron density distribution which can be represented by a Fourier expansion

$$\rho(xyz) = \frac{1}{V}\sum_{hkl} F_{hkl} \cdot e^{-2\pi i[hx+ky+lz]}, \tag{1}$$

where F_{hkl} are the structure factors. The values of the F_{hkl} can be represented as a function of hkl on the reciprocal lattice, Fig. 1(a). If the F_{hkl} are known then $\rho(xyz)$

can be calculated by Eq. (1). Structure factors are usually complex quantities. If they are to be measured by X-ray diffraction, only their absolute values can be obtained. The phases are lost.

The electron density function $\rho(xyz)$ is of limited variance given by the size of an atom. Hence, the F_{hkl} must obey certain internal relationships which can be used to obtain some information about the missing phases. This is the reason why crystal structure analysis is possible at all, even with missing phases.

The absolute values of the structure factors $|F_{hkl}|$ are mostly determined from single crystal diffraction experiments (Klug and Alexander, 1974; Luger, 1980), measuring the reflected intensities, which are proportional to $|F_{hkl}|^2$, in all reciprocal lattice points (up to a reasonable upper limit).

If no single crystals are available, also polycrystal diffraction can be used (Jansen *et al.*, 1992; Baerlocher, 1995; Altomare *et al.*, 1995). A polycrystalline sample

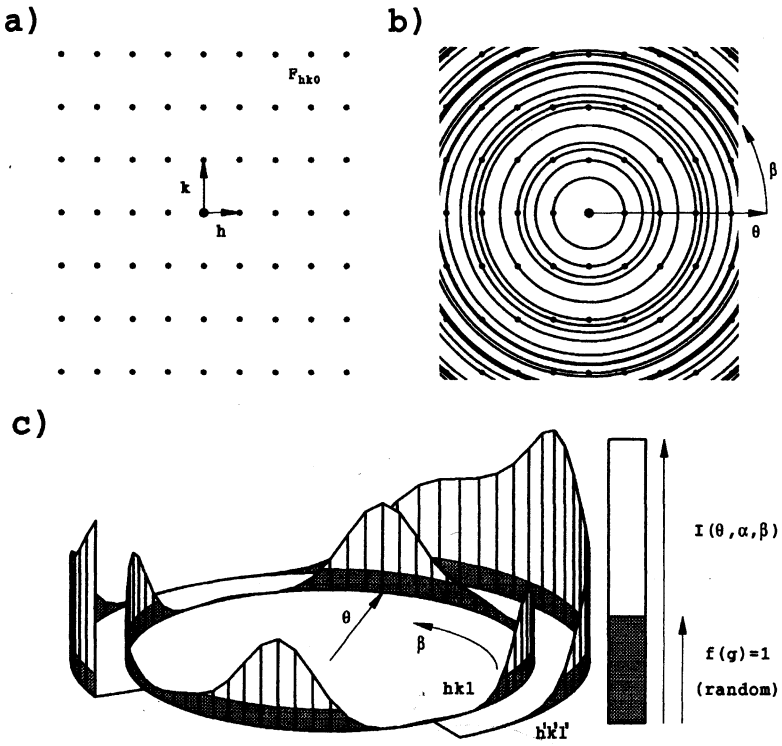

Figure 1 Intensity distribution in the reciprocal space (two-dimensional): (a) reciprocal lattice of a single crystal; (b) the reciprocal lattice points in a polycrystal lie on spheres (or circles); (c) intensity distribution on two such spheres (circles) in a powder with non-random orientation distribution (texture).

consists of (infinitely) many structurally identical single crystals which have, however, different orientations g of their crystal axes. Hence, also their respective reciprocal spaces are rotated through g. Then infinitely many reciprocal lattices are superposed. Hence, the reciprocal space of a polycrystalline sample consists of spheres on which the intensity $|F_{hkl}|^2$ is continuously distributed, Fig. 1(b).

If the orientation distribution of the crystallites is random then the intensity distribution on each sphere is constant, i.e. it is independent of the polar angles $\{\alpha\beta\}$ specifying a point on a sphere. In this case there is a simple relationship between the intensities $|F_{hkl}|^2$ of any *hkl* of a single crystal and the powder diffraction intensities on the spheres.

In crystals with big unit cells there are, however, many "superpositions" of different *hkl*, the spheres of which have the same (or nearly the same) radius. In this case the unique relationship between single crystal intensities and polycrystal intensities cannot be inverted uniquely. This is the essential restricting condition which renders crystal structure analysis from powder diffraction much more difficult than from single crystal diffraction.

If the orientation distribution of the crystallites is not random then the spheres carry intensity distributions which vary with the angles $\alpha\beta$ on the sphere as is shown schematically in Fig. 1(c) for a two-dimensional case (showing only the angle β). Then the *average intensity* on a sphere still corresponds to that in the case of *random powder* and hence to the *single crystal* $|F_{hkl}|^2$. The "variance" on the sphere corresponds to the orientation distribution of the crystallites. If the two spheres *hkl* and $h'k'l'$, shown in Fig. 1(c), happen to have the same radius then the two intensity distributions on them are added. If we know, however, the orientation distribution of the crystallites then the *shapes* of the two intensity functions on $\alpha\beta$ are known. Hence, the superpositions can be deconvoluted if the superposed intensities have been measured as a function of the angles $\alpha\beta$.

This is the principle of crystal structure analysis from *textured* powder samples.

EXPERIMENTAL TECHNIQUE

Single crystal X-ray diffraction is mostly carried out with small single crystals which may be considered as having no extension (compared to the dimensions of the experimental equipment). This situation can practically not be achieved with polycrystalline samples. In X-ray powder diffraction, focusing methods are often preferred which require flat (extended) samples (see e.g. Klug and Alexander, 1974; Bish and Post, 1984; Jenkins and Snyder, 1996).

Powder diffraction with random samples requires the diffraction vector **s** to be oriented only in one direction with respect to the sample. It is then usually chosen perpendicular to the flat sample surface. This allows to use the Bragg–Brentano technique with the sample surface tangent to the focusing circle (or more correctly to the focusing cylinder), Fig. 2(a).

Powder diffraction with non-random (textured) samples requires the diffraction vector **s** to be brought into many orientations $\alpha\beta$ with respect to the sample surface.

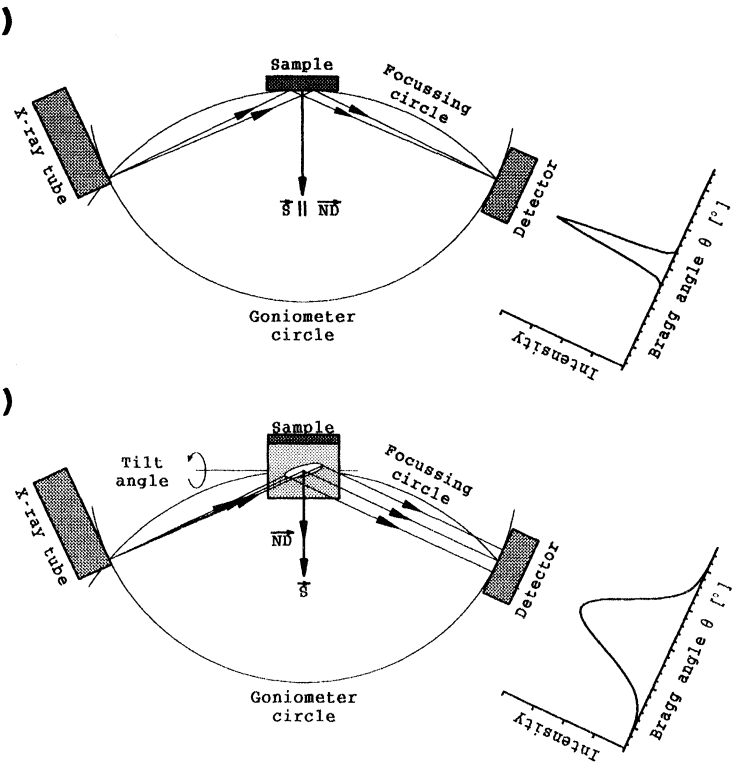

Figure 2 Principles of powder diffractometry using the Bragg–Brentano geometry: (a) the sample in the focused zero-tilt position; (b) the sample tilted by an angle $\alpha = \chi$.

This requires a sample orientation device which is most often chosen in the form of an Eulerian cradle fixed on the $\theta = \omega$ axis of a θ–2θ powder diffractometer. The tilt angle α can then be achieved either by the goniometer angle ω or by the Eulerian cradle angle χ, i.e. by ω-tilt or χ-tilt. The most common method in texture analysis is χ-tilt as is illustrated in Fig. 2(b). This leads to peak broadening due to a violation of the focusing conditions, and this, in turn, leads to abundant peak overlap.

As an example, Fig. 3 shows peak profiles measured with a texture goniometer (Wcislak and Bunge, 1996) at different sample tilt angles α. One sees the strong peak broadening with increasing sample tilt.

Powder diffraction diagrams as they have to be evaluated for crystal structure analysis are shown in Fig. 4. They correspond to a polyoxadiazole derivate used later in the model calculations.

The sample orientation angle β corresponds to a rotation of the sample about its surface normal direction. This rotation does not change the focusing conditions

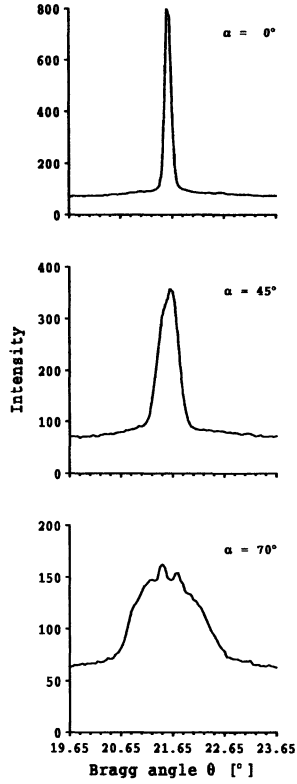

Figure 3 Peak profiles measured in a random copper sample at different tilt angles α.

(respectively the violated conditions). Hence, peak broadening is independent of the angle β.

THE DECONVOLUTION PROBLEM

Under these experimental conditions three-dimensional intensity distribution functions can be measured. They can be expressed in the form

$$I(\theta, \alpha, \beta) = I_0 \cdot C(\theta, \alpha) \cdot \sum_{hkl} |F_{hkl}|^2 \cdot m_{hkl} \cdot B\{\theta - \theta_{hkl}, b(\theta, \alpha)\} \cdot P_{hkl}(\alpha, \beta). \quad (2)$$

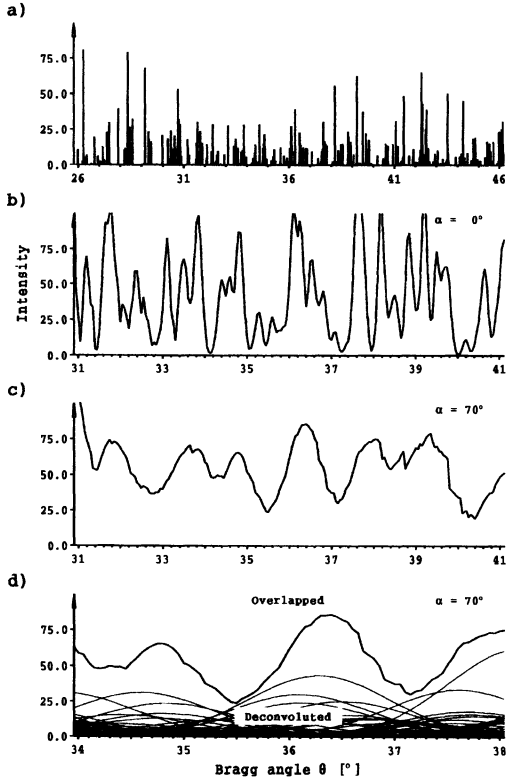

Figure 4 Theoretical powder diffiractograms (polyoxadiazole): (a) the streak diagram; (b) diffraction peaks corresponding to diagram (a) with peak widths according to the focusing sample orientation $\alpha = 0°$; (c) abundantly overlapping diffraction peaks at $\alpha = 70°$; (d) deconvolution of the overlapped peaks.

Thereby I_0 is the primary intensity, $C(\theta, \alpha)$ is an instrumental factor containing, for instance, divergencies and absorption, B is the peak profile function centred at the ideal position θ_{hkl} and having a width described by the parameter b which depends on θ and α, m_{hkl} is the multiplicity (according to crystal symmetry and the form of the hkl) of the reflection hkl, and finally $P_{hkl}(\alpha, \beta)$ is the pole density distribution function (i.e. the pole figure).

The pole distribution functions of the different reflections hkl are not independent of each other. Rather they are integrals over the orientation distribution function $f(g)$ of the crystallites of the sample. It is

$$P_{hkl}(\alpha, \beta) = \frac{1}{2\pi} \int_{hkl \perp \alpha\beta} f(g)\, \mathrm{d}\psi, \quad g = \{\phi_1, \Phi, \phi_2\}. \tag{3}$$

Thereby ψ is the rotation angle about the normal direction to *hkl*, i.e. about the sample direction $\alpha\beta$ and about the diffraction vector **s** (for details see e.g. Bunge, 1993).

Equations (2) and (3) must be considered for two different situations:

- At the beginning of the investigation $|F_{hkl}|$ and $f(g)$ are unknown.
- Later on $f(g)$ has first been determined, then only the $|F_{hkl}|$ remain as unknowns which have to be determined from measured intensity data.

In order to develop an effective deconvolution procedure it is helpful to estimate the expected number of unknowns as well as the number of available experimental input data from which the unknowns are to be calculated.

The number of unknown values $|F_{hkl}|$ is given by the volume of the reciprocal unit cell depending on the reciprocal lattice vectors $\mathbf{a}^*$, $\mathbf{b}^*$, and $\mathbf{c}^*$, the crystal symmetry and the considered range $\theta_{\max}$ of the powder diffraction diagram. The influence of crystal symmetry can be approximated by the multiplicity m_{gen} of the general form. One thus obtains

$$N_{hkl} \approx \frac{(4\pi/3)(\sin\theta_{\max}/\lambda)^3}{[\mathbf{a}^* \cdot \mathbf{b}^* \times \mathbf{c}^*] \cdot m_{\text{gen}}}. \tag{4}$$

In the example considered later with the lattice parameters of Eq. (22) and $\theta_{\max} = 66°$ ($Cu_{K\alpha}$ radiation) this leads to $N_{hkl} = 756$.

The texture $f(g)$ can be represented by its series expansion coefficients $C_\lambda^{\mu\nu}$, Eq. (9), the number of which depends on the "sharpness" of the texture. The texture can be varied deliberately by the experimenter in certain (rather wide) limits. Hence, it is in the hands of the experimenter how many texture coefficients have to be determined. Reasonable ranges may be estimated by

$$0 \leq N_C \leq N_{\max} \sim 500 \tag{5}$$

depending on crystal symmetry (the lower the crystal symmetry the higher is $N_{\max}$).

Thereby it must be taken into consideration that the resolution for $|F_{hkl}|$ is the better the sharper the texture, i.e. the higher the number N_C.

However, since the experimenter is able to choose the texture himself, it is possible to combine different measurements with different degrees of texture sharpness, for instance, starting at first with a sample with a flat texture and then, when some resolution has already been reached, proceeding to another sample prepared from the same powder but now with a sharper texture.

Hence, in the example considered later on, the number of unknowns is in the order of

$$N_{hkl} + N_C \leq 756 + 500 = 1256. \tag{6}$$

The number N_I of measurable intensity data (input data) $I(\theta, \alpha, \beta)$ depends on the resolving power of the used texture goniometer in all three variables $\theta\,\alpha\,\beta$:

$$N_I = N_\theta \cdot N_{\alpha\beta} = \frac{\theta_{\text{range}}}{\Delta\theta} \cdot \frac{x \cdot 2\pi}{\Delta\alpha\,\Delta\beta} \tag{7}$$

thereby θ_{range} is the available θ range, $\Delta\theta$ is the resolving step in θ, x is the measurable part of the pole sphere (i.e. of the hemisphere) and $\Delta\alpha, \Delta\beta$ are the resolved steps in the two pole figure angles $\alpha\beta$.

As an example we may assume the following values:

$$\Delta\theta = 0.05°, \quad \theta_{min} = 6°, \quad \theta_{max} = 66°, \quad \Delta\alpha = \Delta\beta = 5°, \quad x = 0.7; \quad (8)$$

then we obtain

$$N_I = 1200 \cdot 1080 = 1.296 \cdot 10^6 \quad (9)$$

different intensity values.

This shows that the number of experimental data points is by far higher than the number of unknowns, i.e. the number of $|F_{hkl}|$ and $C_\lambda^{\mu\nu}$ together. This may be compared with the situation in "random" powder diffraction. In this case there are no unknown texture coefficients $C_\lambda^{\mu\nu}$ but the number of input data is drastically smaller by the factor $N_{\alpha\beta}$. In the example given above there would remain only $N_I = 1200$ intensity values (assuming the same angular resolution in 2θ) compared with 756 unknowns.

In random powder diffraction, i.e. without the necessity of sample tilt, usually higher angular resolution in 2θ can be achieved, e.g. 0.005°. Then the number of available intensity data would be $N_I = 12000$ in this case.

It must be mentioned that very small angular steps $\Delta\alpha$ and $\Delta\beta$ may lead to "redundant" data which do not carry independent information (depending on the sharpness on the texture).

A DECONVOLUTION PROCEDURE

Equation (2) contains four types of quantities:

- The three-dimensional intensity distribution function $I(\theta, \alpha, \beta)$ as the primary experimental input data.
- The instrumental quantities C, B and b.
- The texture of the sample described by $P_{hkl}(\alpha, \beta)$ or $f(g)$.
- The unknown structure factors $|F_{hkl}|$.

The instrumental quantities are, in principle, independent of the particular studied sample. Hence, they can be assumed to have been measured beforehand. So, they may be assumed to be known in the actual deconvolution.

The texture of the sample is unknown. It is described by a not-too-high number of parameters $C_\lambda^{\mu\nu}$(Eq. (10)). Hence, it can be determined from *parts of the diffraction diagram* with no or only small overlap in θ. In these parts of the diffraction diagram the two types of unknowns, i.e. the texture factors and the structure factors, can easily be separated by employing well-established methods of quantitative texture analysis (see e.g. Dahlem-Klein *et al.*, 1993).

Finally, deconvolution for *all* $|F_{hkl}|$ can be done also in the strongly overlapped parts of the diffraction diagrams but then with already known texture.

TEXTURE DETERMINATION

The texture is expressed in terms of a series expansion (see e.g. Bunge, 1993)

$$P_{hkl}(\alpha,\beta) = \sum_{\lambda=0}^{L} \sum_{\mu=1}^{M(\lambda)} \sum_{\nu=1}^{N(\lambda)} \frac{4\pi}{2\lambda+1} C_{\lambda}^{\mu\nu} \cdot k_{\lambda}^{\mu}(\theta_{hkl},\gamma_{hkl}) \cdot k_{\lambda}^{\nu}(\alpha,\beta). \tag{10}$$

Thereby k_{λ}^{μ} and k_{λ}^{ν} are spherical surface harmonics which are invariant with respect to crystal and sample symmetry, respectively. θ_{hkl} and γ_{hkl} are polar coordinates of the normal direction to the lattice plane (*hkl*) referred to the chosen crystal coordinate system.

The functions $P_{\mathrm{hkl}}(\alpha,\beta)$ are normalized over the whole sphere:

$$\oint_{\alpha\beta} P_{hkl}(\alpha,\beta) \sin\alpha \, \mathrm{d}\alpha \, \mathrm{d}\beta = 4\pi. \tag{11}$$

Also the peak profile functions B are normalized over the peak width

$$\int_{\theta} B\{\theta - \theta_{hkl}, b\} \, \mathrm{d}\theta = 1. \tag{12}$$

Hence, in non-overlapped parts of the diffraction diagram the integral intensities $I_{hkl}^{\mathrm{int}}(\alpha,\beta)$ can be obtained by integrating Eq. (2) over θ (as in Eq. (12)). It is

$$I_{hkl}^{\mathrm{int}}(\alpha,\beta) = I_0 \cdot C(\theta,\alpha) \cdot |F_{hkl}|^2 \cdot m_{hkl} \cdot P_{hkl}(\alpha,\beta). \tag{13}$$

Since the instrumental function C is known, the factor $I_0 \cdot |F_{hkl}|^2 \cdot m_{hkl}$ follows by integrating Eq. (13) over $\alpha\beta$ according to Eq. (11). Then Eq. (13) gives the normalized functions $P_{hkl}(\alpha,\beta)$ from which the coefficients $C_{\lambda}^{\mu\nu}$ can be determined by solving Eq. (10). In this latter equation, $M(\lambda)$ unknowns $C_{\lambda}^{\mu\nu}$ are contained in each of several systems of linear equations (one such system for every combination of indices λ and ν).

Hence, the solution can be obtained if at least $M(\lambda)$ functions $P_{hkl}(\alpha,\beta)$ are known. The numbers $M(\lambda)$ depend on λ and on crystal symmetry. (This procedure corresponds to well-established methods of texture analysis, see e.g. Bunge, 1993.)

It must be mentioned that the solution of Eq. (10) for $C_{\lambda}^{\mu\nu}$ is also possible if $P_{hkl}(\alpha,\beta)$ are not known in the full range of $\alpha\beta$ (incomplete pole figures) so that the normalization condition (11) cannot be used explicitly. Also, the solution is still possible for low-order superpositions of a few *hkl*. The solution procedures for these cases are, however, not described in detail here (for details see e.g. Dahlem-Klein *et al.*, 1993).

DETERMINATION OF $|F_{hkl}|$

Once the texture is known, the $P_{hkl}(\alpha, \beta)$ in Eq. (2) are known for all hkl and all $\alpha\beta$. Hence, only the $|F_{hkl}|^2$ remain unknown in this equation. Then Eq. (2) can be written in the form

$$I(\theta, \alpha, \beta) = \sum_{hkl} |F_{hkl}|^2 \cdot A_{hkl}(\theta, \alpha, \beta). \tag{14}$$

This is a system of linear equations with the unknowns $|F_{hkl}|^2$ and the coefficients $A_{hkl}(\theta, \alpha, \beta)$.

For any given hkl these coefficients $A_{hkl}(\theta, \alpha, \beta)$ become zero for $|\theta - \theta_{hkl}| > \frac{1}{2}\Delta\theta_{\max}$ as is illustrated in Fig. 5(b).

This fact can be used for an approximative, successive least-squares solution (Bronstein and Semendjajew, 1991) as is illustrated in Fig. 5(d) (Hedel *et al.*, 1994).

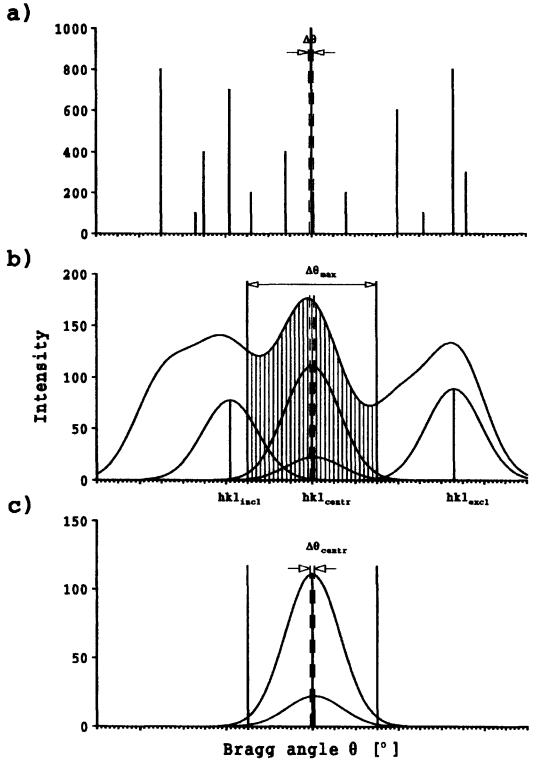

Figure 5

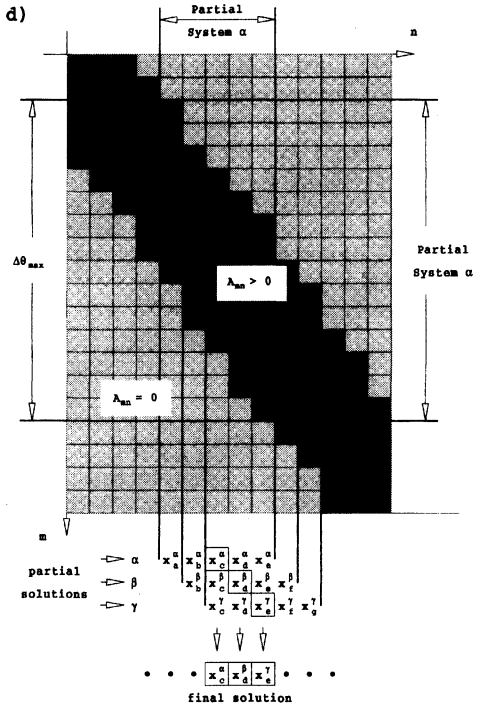

Figure 5 Illustration of the approximative, successive deconvolution procedure: (a) peak positions of the *hkl*, the experimental measuring step $\Delta\theta$ (two peaks lie within this step); (b) the interval $\Delta\theta_{\max}$, the included and excluded *hkl* values hkl_{incl} hkl_{excl} and the central *hkl* value hkl_{centr} (two in this case); (c) the peak profiles of the two *hkl* values the position of which fall into $\Delta\theta_{\max}$; (d) the system of linear equations (16) and its approximative solutions; the partial system α as well as other partial systems β and γ.

For this purpose, Eq. (14) is discretized in steps $\Delta\theta, \Delta\alpha, \Delta\beta$ for which experimental intensity values were measured:

$$\begin{aligned} &\theta_{\min} \leq m_1 \cdot \Delta\theta \leq \theta_{\max}, \\ &\alpha_{\min} \leq m_2 \cdot \Delta\alpha \leq \alpha_{\max}, \\ &\beta_{\min} \leq m_3 \cdot \Delta\beta \leq \beta_{\min}, \qquad m = \{m_1\, m_2\, m_3\}. \end{aligned} \tag{15}$$

Numbering successive *hkl* values by the index n, Eq. (14) can be further shortened in the form

$$I_m = A_{mn} \cdot x_n, \quad x_n = |F_{hkl}|_n^2, \quad x_n > 0. \tag{16}$$

The matrix A_{mn} is illustrated schematically in Fig. 5(d).

Then a *partial* system of equations can be selected out of the full system containing only θ values out of an interval $\Delta\theta_{max}$, wide enough to contain the full width of the central peak hkl_{centr}. This system contains only the unknowns $|F_{hkl}|^2$ the diffraction peaks of which contribute intensity to the chosen θ interval. They are indicated in Fig. 5(b) by hkl_{incl}. The ones which do not contribute intensity to this interval are excluded hkl_{excl}. (In fact, these unknowns are multiplied by $A_{hkl}(\theta, \alpha, \beta) = 0$ in Eqs. (13) and (16).) This partial system is then solved for the $|F_{hkl}|^2_{incl.}$ including the positivity condition of Eq. (16). If x_n turns out to be negative it is put to zero. For the final solution only those hkl are kept which lie inside the *central* interval $\Delta\theta_{centr}$, Fig. 5(b) (which has the size of one experimental step in θ).

This procedure is repeated for all intervals $\Delta\theta$ between θ_{min} and θ_{max} taken as $\Delta\theta_{centr}$. After that, solutions for *all* $|F_{hkl}|^2$ have been obtained as is shown schematically in Fig. 5(b).

EXACT SUPERPOSITIONS

The described deconvolution procedure is essentially based on the resolving power of texture measurement in the sample rotation angles $\alpha\beta$. It is able to resolve superpositions of hkl in the Bragg angle θ which are closer than the experimental step $\Delta\theta$ and, even more so, with respect to the width b of the profile function B. In fact, the width b of the profile functions in *texture analysis* is often higher than that used in *high-resolution powder diffraction*. The *loss* of resolving power in θ is, however, *by far overcompensated* by the *gain* of information (and resolving power) according to the sample angles $\alpha\beta$.

Equation (14) shows very clearly the increase of the number of equations due to the variables $\alpha\beta$ compared with the situation in random powders where only one intensity value is available for each value θ (see e.g. the example given in Eq. (9)).

From the above-said it follows that the deconvolution of superposed *hkl does not depend on their distance in* θ. In fact, even *hkl* having *exactly the same* θ *value* may be deconvoluted in the same way. *Systematic* superpositions of this type occur, for instance, in cubic crystal symmetry where all reflections with the same sum $h^2+k^2+l^2$ have *exactly* the same θ_{hkl}. (As an example, this is the case for 621, 540, 443 in a cubic primitive lattice.) The deconvolution procedure is thus able to deconvolute also such *exact* coincidences in the same way as *nearly* coincident reflections.

TEST OF THE DECONVOLUTION PROCEDURE BY MODEL CALCULATIONS

In order to test the deconvolution procedure, it was applied to theoretically constructed intensity distributions Eq. (2) assuming $|F_{hkl}|^2$ according to a known crystal structure. Also the texture of the sample was assumed to be known. Particularly we used textures consisting of several preferred orientations g_i with

Gaussian spread about them together with a random component

$$f(g) = v_0 + \sum_i v_i \cdot e^{-\left|\Delta g/\omega_i\right|^2}, \quad g = \Delta g \cdot g_i. \tag{17}$$

Thereby v_i are the volume fractions of the components, Δg is the distance from the preferred orientation and ω_i characterizes the spread width. The coefficients $C_\lambda^{\mu\nu}$ of one of these components can be easily written in the form

$$C_\lambda^{\mu\nu} = \frac{\exp\{-(1/4)\lambda^2\omega_i^2\} - \exp\{-(1/4)(\lambda+1)^2\omega_i^2\}}{1 - \exp\{-(1/4)\,\omega_i^2\}} \cdot \dot{\dot{T}}_\lambda^{\mu\nu}(g_i). \tag{18}$$

The deconvolution procedure was tested by comparing input and output texture coefficients $C_\lambda^{\mu\nu}$ in terms of an accuracy measure R_C:

$$R_C = \frac{\sum_{\lambda\mu\nu} \left|C_\lambda^{\mu\nu}(\text{input}) - C_\lambda^{\mu\nu}(\text{output})\right|}{\sum_{\lambda\mu\nu} \left|C_\lambda^{\mu\nu}(\text{input})\right|}. \tag{19}$$

As the final result of the deconvolution procedure, the input and output structure factors were compared by the accuracy measure R_F:

$$R_F = \frac{\sum_{hkl} \left|\left|F_{hkl}^{\text{in}}\right|^2 - \left|F_{hkl}^{\text{out}}\right|^2\right|}{\sum_{hkl} \left|F_{hkl}^{\text{in}}\right|^2}. \tag{20}$$

The intensity function (2) contains the peak profile function $B\{\theta - \theta_{hkl}, b\}$ which fully enters the coefficients A_{hkl} in Eq. (14). Hence, the type of this function and the width $b(\theta, \alpha)$ must be considered *with the highest possible accuracy*. The function depends on the particular features of the used diffractometer. In the present case, it was found that peak profiles for all θ and α could be best represented by a pseudo-Voigt function (see e.g. Wcislak and Bunge, 1996)

$$\begin{aligned} B(\theta) &= \eta \cdot B^{\text{Gauss}}(\theta) + (1-\eta) \cdot B^{\text{Cauchy}}(\theta), \\ B^{\text{Gauss}}(\theta) &= B_{\max} \cdot e^{-\left(\Delta\theta/\sigma\right)^2}, \qquad \Delta\theta = \theta - \theta_{hkl}, \\ B^{\text{Cauchy}}(\theta) &= B_{\max} \frac{1}{1 - \left(\Delta\theta/\sigma\right)^2}, \end{aligned} \tag{21}$$

where η is a "shape parameter" and the width σ depends on θ and α.

For modelling purposes it is sufficient to assume $\eta = 1$. For real measurements, of course, the experimental function must be used (see e.g. Wcislak and Bunge, 1996).

Numerical calculations were carried out assuming structure factors (Kraus and Nolze, 1996) of an orthorhombic polyoxadiazole derivate with

$$a = 36.468\,\text{Å}, \qquad b = 6.974\,\text{Å}, \qquad c = 6.030\,\text{Å}, \tag{22}$$

and the space group $C2_1mc$. Measurements were simulated in steps of

$$\Delta\theta = 0.05°, \qquad \Delta\alpha = \Delta\beta = 5°$$

in the intervals

$$6° \leq \theta \leq 66°, \qquad 0° \leq \alpha \leq 70°, \qquad 0° \leq \beta \leq 360° \tag{23}$$

assuming orthorhombic sample symmetry.

For the first step of the procedure, i.e. texture determination, two variants were considered (Hedel *et al.*, 1996):

(a) only the non-overlapped reflections (pole figures)
600, 310, 510, 111, 311, 710, 511, 910, 020, 711, 220, 002
were used;
(b) the single and two-fold overlapped pole figures
310 + 600, 111 + 800, 511, 311 + 710, 1000, 020 + 910, 220 + 711, 202 + 221, 421 + 402
were combined.

The overlapping factors of the two-fold overlapped reflections were determined simultaneously during texture determination (Dahlem-Klein *et al.*, 1993). The series expansion degree was $L = 22$ in case (a) (with twelve pole figures) and $L = 16$ in case (b) (with nine pole figures).

Hypothetical textures but with realistic features were composed of the ideal orientations given in Table 1.

RESULTS

At first the accuracy of texture determination was tested using a texture consisting of the components listed in Table 1.

In Fig. 6 input and output pole figures are compared. Those of Fig. 6(a) were used for texture determination case (a) and those of Fig. 6(b) were not used. It is seen that the agreement between input and output pole figures for both groups is reasonably good at least considered at a qualitative level.

Figure 7 compares input and output texture in terms of the accuracy parameter R_C. The starting texture was that according to no. 5 in Table 1.

In Fig. 7(a) the texture sharpness was varied by varying the spread width of the components. Curve a in this figure corresponds to only non-overlapped pole figures whereas curve b includes two-fold overlapped ones. It is seen that in case (a) the accuracy increases with increasing spread width whereas in case (b) it decreases. This latter fact can be understood since with decreasing texture sharpness (i.e. increasing

Table 1 Some textures composed of ideal orientations g_i specified by their Euler angles ϕ_1, Φ, ϕ_2 and their respective volume fraction

S. No.	*Texture*	ϕ_1 [°]	Φ [°]	ϕ_2 [°]	*Fraction* [%]
1	Single component	0	0	0	100
2	Two components	90	90	0	63.33
		70	90	0	21.66
3	Three components	0	0	0	21.66
		0	90	90	21.66
		90	90	0	21.66
4	Fibre texture	0	90	0	5.00
		0	90	5	5.00
		0	90	10	5.00
		0	90	15	5.00
		⋮	⋮	⋮	⋮
		0	90	90	5.00
5	Multi component	0	70	0	1.50
		20	0	0	1.50
		40	0	0	1.50
		0	45	0	14.30
		20	45	0	14.30
		40	45	0	14.30
		0	75	20	7.10
		0	75	40	7.10
		20	55	20	4.30
		40	55	40	4.30
	All textures	Fraction of the random distribution: 5.0% Spread width of the texture components: 15°			

half width) the determination of the overlapping factors of the pole figures becomes increasingly difficult.

Figure 7(b) shows similar results as a function of the random fraction. Since here the sharpness of the individual texture components remains constant curves a and b are nearly identical.

Next, the total deconvolution procedure was tested by comparing input and output $|F_{hkl}|$ values. The used deconvolution method is an approximation depending on the size of the interval $\Delta\theta_{max}$ according Fig. 5. Hence, the size of this interval was varied. The result is shown in Fig. 8. It is seen that the accuracy converges to a constant value above $\Delta\theta_{max} \sim 0.45°$. Hence, in the following, lower values of $\Delta\theta_{max}$ were no more used.

The quality of the approximation, illustrated in Fig. 5, can also be judged by Fig. 9. Here the solutions of the partial systems (for the same unknown $x_n = |F_{hkl}|_n^2$) are plotted as a function of θ of the central interval of the partial system. The central value of Fig. 9 was then kept for the total solution. If the partial solutions were exact, then they should be identical, so that Fig. 9 were a straight horizontal line. Hence, the deviation from the straight line illustrates the degree of accuracy obtained by the approximative nature of the solution. Also the absolute deviation of the solution from the theoretical (input) value can be seen.

The accuracy of the deconvolution procedure also depends on the type of texture, i.e. how many texture components it contains. This is shown in Fig. 10. In this figure

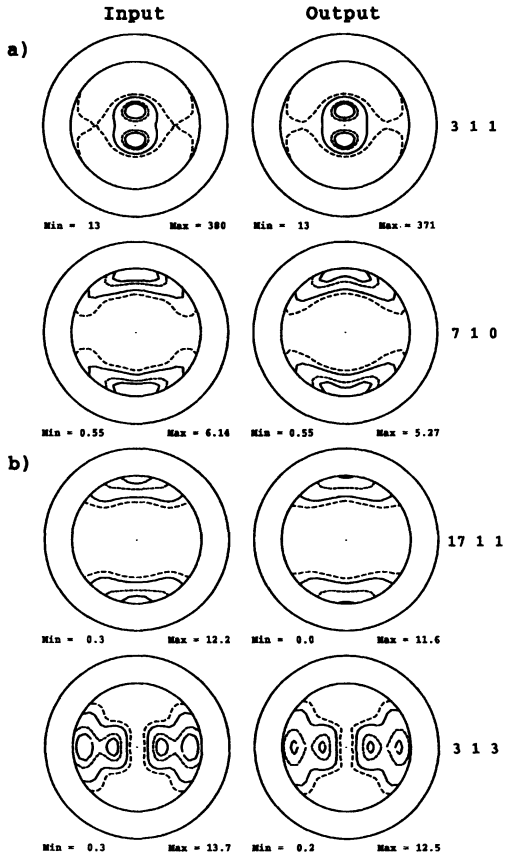

Figure 6 Input and output pole figures (texture according to Table 1, no. 5): (a) pole figures used for the determination of the texture coefficients $C_\lambda^{\mu\nu}$; (b) pole figures not used to determine $C_\lambda^{\mu\nu}$.

the deconvolution for the $|F_{hkl}|$ values was done using, in the second step, either the theoretical input texture or the texture obtained from the first step of the procedure. It is seen that the deconvolution works extremely well when the texture is exactly known. The essential part of error is due to the errors introduced through the uncertainty of texture determination. (In Fig. 10 the "sharpness" of the texture is expressed in terms of the "texture index", see e.g. Bunge, 1982.)

The same trend can be seen when the texture sharpness is varied either by the spread width of the texture components, Fig. 11(a), or by the random component, Fig. 11(b). In both figures the use of the ideal input texture allows a very accurate deconvolution of the overlapped peaks. If retrieved textures are used, the results

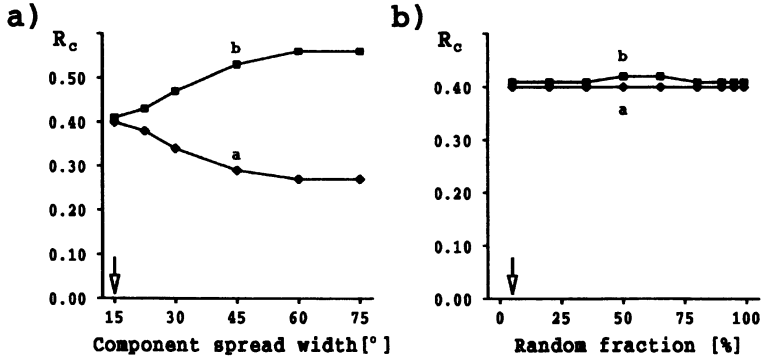

Figure 7 Discrepancy values R_C as a function of texture sharpness: curve a: only non-overlapped pole figures were used; curve b: single and two-fold overlapped pole figures were used; (a) R_C as a function of the spread width; (b) R_C as a function of the random fraction. The multi-component texture (no. 5, Table 1) was used as starting texture, indicated by ↓ in the diagrams.

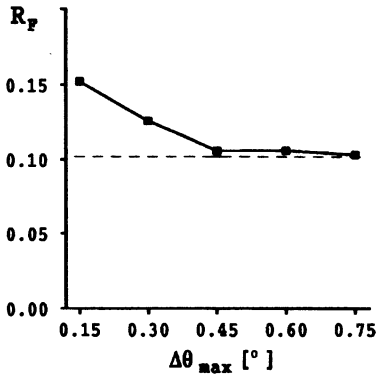

Figure 8

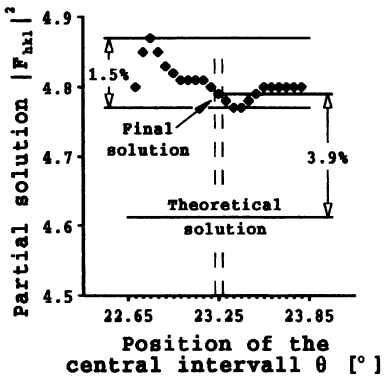

Figure 9

Figure 8 Influence of the size of the interval $\Delta\theta_{max}$ (see Fig. 5) on the accuracy of deconvolution of the $|F_{hkl}|$. Texture according to Table 1, no. 5.
Figure 9 Solution for the same structure factor $|F_{hkl}|$ in neighbouring partial equation systems characterized by the position in θ of their central interval $\Delta\theta_{centr}$.

from isolated peaks alone are much better than with included overlapped ones. Both figures also show that deconvolution is no more possible (even with the ideal texture) when the texture approaches the random distribution (as is evident from the general considerations given above).

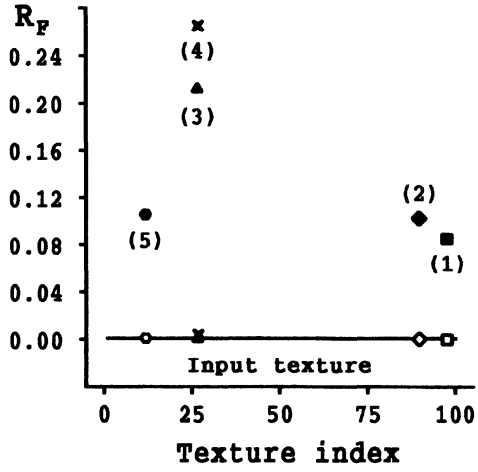

Figure 10 Influence of the type of texture (Table 1) on the accuracy of deconvolution: $\Delta\theta_{max}$ 0.75° and lattice constant a according to Eq. (22).

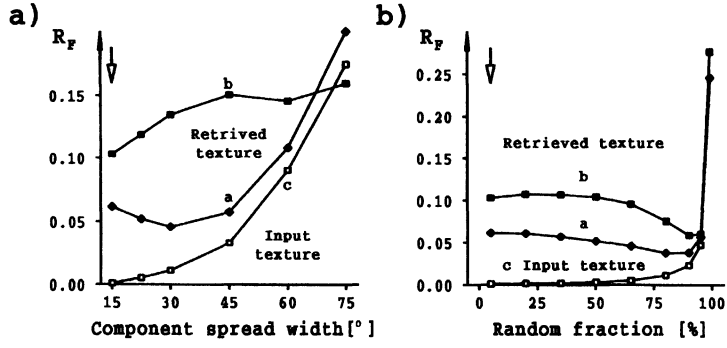

Figure 11 Discrepancy values R_F as a function of texture sharpness: curve a: only non-overlapped pole figures were used; curve b: single and two-fold overlapped pole figures were used; curve c: the theoretical input texture was used; (a) R_F as a function of the spread width; (b) R_F as a function of the random fraction. The multi-component texture (no. 5, Table 1) was used as starting texture, indicated by ↓ in the diagrams, $\Delta\theta_{max}$ 0.75° and lattice constant a according to Eq. (22).

It is interesting to know, how experimental errors in the measurement of diffraction spectra influence the results. Figure 12(a) shows the influence of a shift of the whole diffraction diagram, i.e. the peak profile function of each peak is shifted out of its centre. In Fig. 12(b) the influence of a wrong peak width b is illustrated. These two figures give an impression of the required experimental accuracy.

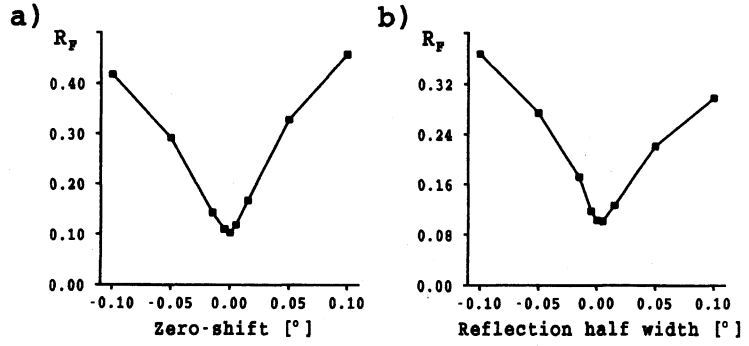

Figure 12 Discrepancy values R_F as a function of systematic experimental errors: (a) as a function of zero-shift of the whole diffraction diagram; (b) as a function of an error in the half-width of the peak profile function.

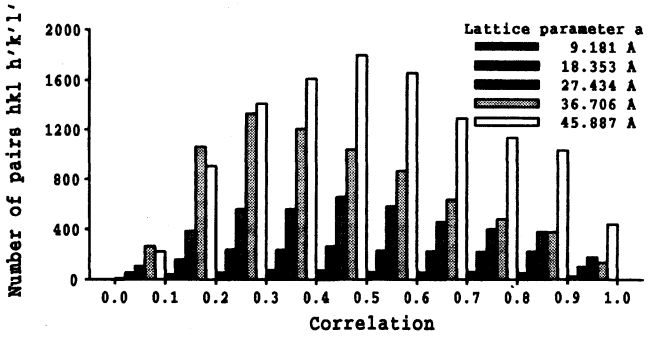

Figure 13 The number of reflections *hkl* showing a particular correlation value with respect to their neighbouring overlapped reflections $h'k'l'$.

From Fig. 7, curves b, it was evident that a great deal of uncertainty is introduced into texture analysis by the uncertainty of overlapping factors obtained by the used algorithm of texture analysis, i.e. the iterative series expansion method (Dahms and Bunge, 1989).

In order to quantify the "degree of overlap", illustrated in Fig. 4, a correlation factor $\mathrm{Corr}_{hkl,\,h'k'l'}$ of the two reflections *hkl* and $h'k'l'$ was introduced:

$$\mathrm{Corr}_{hkl,\,h'k'l'} = \frac{\Sigma_\theta \Sigma_\alpha \Sigma_\beta I_{hkl} \cdot P_{hkl}(\alpha,\beta) \cdot B(\theta, b(\theta,\alpha)) \cdot I_{h'k'l'} \cdot P_{h'k'l'}(\alpha,\beta) \cdot B(\theta, b(\theta,\alpha))}{\sqrt{\Sigma_\theta \Sigma_\alpha \Sigma_\beta I_{hkl}^2 \cdot P_{hkl}^2(\alpha,\beta) \cdot B^2(\theta, b(\theta,\alpha))} \cdot \sqrt{\Sigma_\theta \Sigma_\alpha \Sigma_\beta I_{h'k'l'}^2 \cdot P_{h'k'l'}^2(\alpha,\beta) \cdot B^2(\theta, b(\theta,\alpha))}}. \quad (24)$$

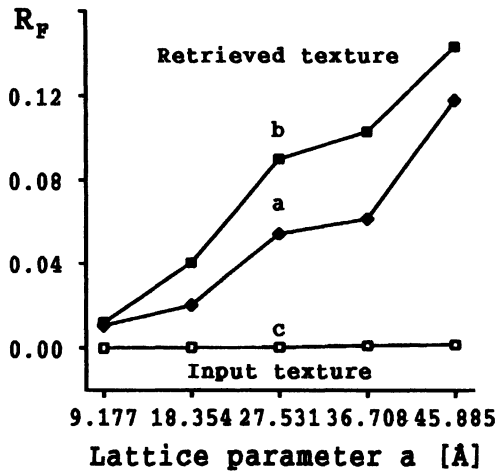

Figure 14 The discrepancy value R_F as a function of an assumed lattice parameter a (the parameters b and c according to Eq. (22)): curve a: only non overlapped pole figures were used; curve b: single and two-fold overlapped pole figures were used; curve c: the theoretical input texture was used.

This factor considers overlap in all three angles $\theta\alpha\beta$. Hence, it depends on the actual texture. The correlation factor can vary between zero and one.

In Fig. 13 the distribution of the reflections hkl according to their correlation factors with respect to neighbouring reflections $h'k'l'$ is shown. The different symbols correspond to different assumed values of the lattice parameter 'a' (compared to that of Eq. (22), with b and c fixed).

It is seen that the number of non-overlapped or only moderately overlapped pole figures decreases drastically with increasing lattice constants.

Finally Fig. 14 shows the accuracy parameter R_F as a function of the assumed lattice parameter 'a'. It is seen that the accuracy decreases with increasing lattice parameter due to the uncertainty in texture determination as a consequence of pole figure overlap. If the texture is exactly known (i.e. the input texture is used) then deconvolution according to Eq. (16) reaches a very high degree of accuracy (curve c).

The accuracy parameters (19) and (20) compare input and output parameters $|F_{hkl}|^2$ and $C_\lambda^{\mu\nu}$ in a global way, i.e. they are averages over all hkl, respectively all $\lambda\mu\nu$. For the final structure analysis, however, the individual and particularly the maximal deviations are even more important.

In Fig. 15 the deconvoluted structure factors $|F_{hkl}|$ are plotted versus their theoretical input values. In this representation the individual errors can be seen directly as deviations of the representing points from the straight line. In order to estimate the accuracy of the retrieved $|F_{hkl}|$ values, the maximum error value is compared with the maximum $|F_{hkl}|$ value. This determines the boundary lines corresponding to relative errors of 9%, 8% and 0.3% of the maximum, respectively.

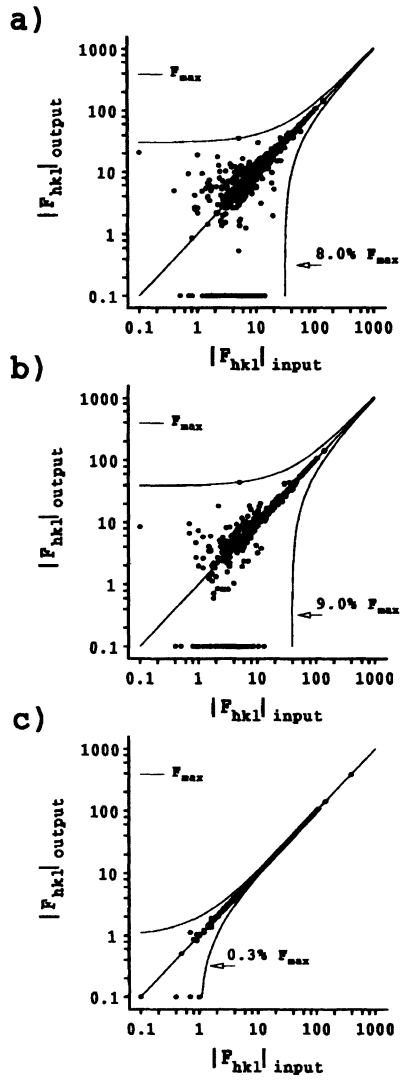

Figure 15 Relationship of generated and deconvoluted structure factors $|F_{hkl}|$: (a) texture retrieved from single and superposed pole figures; (b) texture retrieved only from single pole figures; (c) input texture.

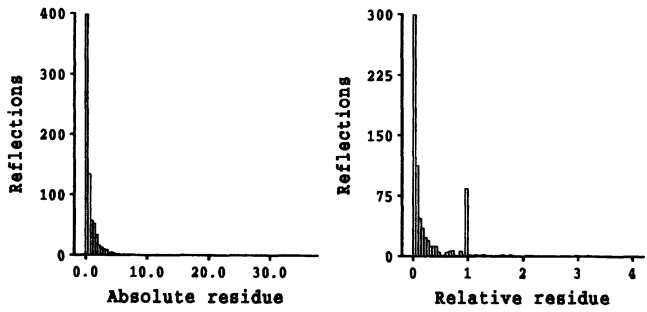

Figure 16 Number of reflections as a function of the absolute and relative residue between $|F_{hkl}|$ input and $|F_{hkl}|$ output.

This representation also shows the $|F_{hkl}|$ values which obtained negative solutions. They were put to zero. In the logarithmic scale of Fig. 15 they are plotted at the lower limit of the diagram. If the deconvolution is done with the theoretical input texture, Fig. 15(c), then the retrieved $|F_{hkl}|$ values have a very high accuracy in the order of 0.3% of the maximum value. In this case no negative values were obtained in the solution. This illustrates again that the by far largest part of the errors comes through texture determination in the first step of the procedure.

The distribution of the residues between input and output $|F_{hkl}|$ is shown in Fig. 16. The absolute values follow approximately a normal distribution. In the distribution of the relative residues, the ones put to zero are seen as a separate "population" in this curve.

CONCLUSIONS

Crystal structure analysis is based on absolute values of structure factors $|F_{hkl}|$. It does not matter how these values were determined. Three methods may be distinguished:

- from single crystals,
- from powders with preferred orientations (texture),
- from random powders.

In single crystals all *hkl* are well resolved in the reciprocal space (except for materials with extremely high lattice parameters such as proteins). In the two powder methods an increasing degree of overlap on the pole spheres $\alpha\beta$ occurs when going from sharp textures to random orientation distribution. Hence, going in the opposite direction from random powders to sharper and sharper textures, an increasing number of superpositions of *hkl* can be deconvoluted using the method described in this paper.

According to practical reasons a two-step procedure was used, calculating, in the first step, the texture of the sample from reflections with either no superposition or at

least only low-order superposition. Model calculations have shown that the deconvolution of reflections *hkl* in the second step can be done with very good accuracy when the texture is correctly known. The essential part of uncertainty comes in through the uncertainty of texture determination from a limited number of reflections and/or a limited number of sample orientations $\alpha\beta$. The uncertainty is higher the higher the degree of superposition of reflections in this first step.

From these results it can be concluded that structure factor determination with an error value of, say, 5% should be possible in structures with lattice parameters at least up to the ones used in the present example.

Texture determination was modelled assuming conditions as they are usual in conventional texture analysis. The model calculations show that this is not yet optimal for the purpose of crystal structure analysis. They show, however, also that the assumed conditions of texture analysis are still far from their theoretically possible limits of accuracy. Hence, it can be estimated in which way the experimental conditions must be changed in order to improve the accuracy of structure factor determination.

Provided such experimental conditions can be established, it should be possible to determine $|F_{hkl}|$ values from textured powder samples with accuracies better than 5% for a reasonably wide class of structures.

Strictly speaking, the determination of structure factors from textured powders should bear the capability of reaching the highest accuracy compared to both other methods, i.e. single crystals and random powders.

On the one hand, a powder represents a much better statistical average than a small single crystalline individuum which may contain unknown lattice imperfections.

On the other hand, the orientation distribution function of the crystallites in the powder is fully taken into consideration. Hence, the uncertainties due to non-random orientation distribution, as they may enter "random powder diffraction", are avoided in this method.

Acknowledgement

The authors gratefully acknowledge sponsoring of this project by the German Research Foundation DFG.

References

Altomare, A., Burla, M. C., Cascarano, G., Giacovazzo, C., Guagliardi, A., Moliterui, A. G. G. and Polidori, G. (1995). Extra: A program for extracting structure-factor amplitudes from powder diffraction data. *J. Appl. Cryst.* **28**, 842–846.

Baerlocher, Ch. (1995). EXTRACT, a FORTRAN program for the extraction of integrated intensities from powder data, Institute of Crystallography, ETH Zurich, Switzerland.

Bish, D. L. and Post J. E. (Eds.) (1984). Modern Powder Diffraction. *Reviews in Mineralogy*, Vol. 20, Mineralogical Society of America, Washington, DC.

Bronstein, I. N. and Semendjajew, K. A. (1991). Taschenbuch der Mathematik Verlag Nauka Moskau and B. G. Verlagsgesellschaft Stuttgart, Leipzig.

Bunge, H. J. (1982). *Texture Analysis in Materials Science*. Butterworths Publ. London. 2nd Ed. (1993) Cuvillier Verlag, Göttingen.

Dahlem-Klein, E., Klein, H. and Park, N. J. (1993). *Program System ODF Analysis*. Cuvillier Verlag, Göttingen.

Dahms, M. and Bunge, H. J. (1989). The iterative series expansion method for quantitative texture analysis. *J. Appl. Cryst.* **22**, 439–447.

Hedel, R., Bunge, H. J. and Reck, G. (1994). A new method for crystal structure analysis of textured samples. In *Texture of Materials ICOTOM-10, Materials Science Forum*, **157–162**, 2067–2074.

Hedel, R., Bunge, H. J. and Reck, G. (1996). Model calculations of intensity deconvolution from textured powder diagrams. In *Textures of Materials ICOTOM-11*, International Academic Publishers, Beijing. 1435–1442.

Jansen, J., Peschar, R. and Schenk, H. (1992). On the determination of accurate intensities from powder diffraction data. *J. Appl. Cryst.* **25**, 231–243.

Jenkins, R. and Snyder, R. L. (1996). *X-Ray Powder Diffractometry*. Wiley-Interscience Publication.

Klug, H. P. and Alexander, L. E. (1974). *X-Ray Diffraction Procedure*. Wiley, New York.

Kraus, W. and Nolze, G. (1996). POWDER CELL – A program for the representation and manipulation of crystal structures and calculation of the resulting X-ray powder pattern. *J. Appl. Cryst.* **29**, 301–302.

Luger, P. (1980). *Modern X-Ray Analysis on Single Crystals*. Walter de Gruyter, Berlin, New York.

Reck, G., Crystal Structure of Polyoxadiazole Derivatives, in preparation.

Wcislak, L. and Bunge, H. J. (1996). *Program System Texture Analysis with a Position Sensitive Detector*. Cuvillier Verlag, Göttingen.